energies

MDPI

Article

Analysis of Natural and Power Plant CO_2 Emissions in the Mount Amiata (Italy) Volcanic–Geothermal Area Reveals Sustainable Electricity Production at Zero Emissions

Alessandro Sbrana [1,*], Alessandro Lenzi [2], Marco Paci [2], Roberto Gambini [3], Michele Sbrana [4], Valentina Ciani [4] and Paola Marianelli [1,*]

[1] Dipartimento di Scienze della Terra, Pisa University, via Santa Maria 53, 56126 Pisa, Italy
[2] Enel Green Power S.p.a., via Andrea Pisano 120, 56126 Pisa, Italy; alessandro.lenzi@enel.com (A.L.); marco.paci@enel.com (M.P.)
[3] RE&E, Rethinking Energy and Environment, 00184 Rome, Italy; geol.roberto.gambini@gmail.com
[4] Terra Energy S.r.l., via Lenin 132, 56017 San Giuliano Terme, Italy; m.sbrana@terra-energy.it (M.S.); ciani@terra-energy.it (V.C.)
* Correspondence: alessandro.sbrana@unipi.it (A.S.); paola.marianelli@unipi.it (P.M.)

Abstract: Geothermal energy is a key renewable energy for Italy, with an annual electric production of 6.18 TWh. The future of geothermal energy is concerned with clarity over the CO_2 emissions from power plants and geological contexts where CO_2 is produced naturally. The Mt. Amiata volcanic–geothermal area (AVGA) is a formidable natural laboratory for investigating the relative roles of natural degassing of CO_2 and CO_2 emissions from geothermal power plants (GPPs). This research is based on measuring the soil gas flux in the AVGA and comparing the diffuse volcanic soil gas emissions with the emissions from geothermal fields in operation. The natural flux of soil gas is high, independently from the occurrence of GPPs in the area, and the budget for natural diffuse gas flux is high with respect to power plant gas emissions. Furthermore, the CO_2 emitted from power plants seems to reduce the amount of natural emissions because of the gas flow operated by power plants. During the GPPs' life cycle, CO_2 emissions in the atmosphere are reduced further because of the reinjection of gas-free aqueous fluids in geothermal reservoirs. Therefore, the currently operating GPPs in the AVGA produce energy at a zero-emission level.

Keywords: Amiata; CO_2 soil flux; CO_2 power plant emission; geothermics; sustainability

Citation: Sbrana, A.; Lenzi, A.; Paci, M.; Gambini, R.; Sbrana, M.; Ciani, V.; Marianelli, P. Analysis of Natural and Power Plant CO_2 Emissions in the Amiata Volcanic–Geothermal Area Reveals Sustainable Electricity Production at Zero Emissions. *Energies* **2021**, *14*, 4692. https://doi.org/10.3390/en14154692

Academic Editor: João Fernando Pereira Gomes

Received: 13 June 2021
Accepted: 27 July 2021
Published: 2 August 2021

1. Introduction

Mt. Amiata is a Pleistocene silicic dome field volcano [1,2] located in southern Tuscany (Italy) in the peri-Tyrrhenian margin of the Apennine chain. The Mt. Amiata volcanic–geothermal area (AVGA) is characterized by a heavy thinning of the continental crust [3], intense crustal extension [4,5], pluton emplacement at shallow crustal levels [6–8], hydrothermal Hg ore deposits [9,10], and high heat-flow values 150–200 mW/m^2 [11]. A high-enthalpy geothermal resource in the AVGA has been well known since the 1960s [12]. Geothermal energy is used for power generation in the geothermal fields of Bagnore and Piancastagnaio, located SW and SE of the volcanic massif, respectively, with a total installed capacity of 121 MW which represented 18% of the total geothermal electricity production in Italy [13]. Natural CO_2-rich gas emissions [14,15], diffuse gas emissions from soil [16], and gas-rich thermal and cold springs are widespread; however, AVGA is part of the Tuscan degassing area, one of the most intense areas of CO_2 degassing of the Earth due to its geodynamic framework.

This paper improves the quantitative assessment of the natural CO_2 emissions in the Mt. Amiata region, widening the soil CO_2 flux survey presented in Sbrana et al. [16] to

cover an overall area of about 280 km^2. The new survey allows to delimit the preferential natural degassing areas of the Mt. Amiata geothermal system. Furthermore, CO_2 soil flux data highlight the relationship between natural and geothermal power plants (GPPs) CO_2 emissions. The role of CO_2 emission in GPPs (an average of around 500 g/kWh is measured in Amiata geothermal fields) is particularly important for the Tuscany region.
Geothermal energy currently provides 31% of the region's electricity needs and can, because of the wide potential of the existing geothermal resources, significantly increase (double up) Tuscany's share of geothermal renewable electricity in 2030–2050. The collected data on natural CO_2 soils emissions demonstrate for the first time that the emissions of power plants are a small part (<8%) of natural total CO_2 emissions. Results of this study are very significant because could demonstrate that geothermal energy is really a green sustainable renewable energy with 0 emissions of CO_2 in atmosphere and therefore strongly contributes to the reduction of greenhouse gas in the atmosphere and consequently significantly to the climate changes mitigation.

2. Geological, Hydrogeological, and Geothermal Settings

The AVGA is dominated by the presence of a Quaternary volcanic complex lava dome field massif (231–305 ka) [2], which is emplaced on the structural high geology of Mt. Amiata–Mt. Razzano in correspondence with a sinistral transcurrent fault. To the east of the volcano, the Radicofani graben develops with a homonymous trachybasaltic volcano in the center. A remarkable uplift (about 800–900 m) affected the volcanic geothermal area because of the isostatic deformations of the low-density granitic bodies from an intrusion/magma chamber seated at about 4–5 km depth. Vertical normal faults separate the Mt. Amiata structural high from the deep Neogene basin. The southern Tuscany succession created by phyllites from a metamorphic basement and by the tectonic sedimentary covers characterizes the area [17].

The subsoil of this volcanic geothermal system is well known because of the deep wells that allow the geothermal fluid production of the Mt. Amiata geothermal fields. The Quaternary magmatism induces a very strong shallow thermal anomaly because of the superimposition of the high regional heat flow due to the regional Plio-Quaternary stretching, local Pleistocene regional intrusions, and fluid convection in shallow fractured geothermal reservoirs in the upflow areas of Piancastagnaio–Bagnore and in correspondence with the main fault systems. Surface thermal manifestations, thermal springs, concentrated gas emissions, and general diffuse natural soil gas emissions, mainly of CO_2, are ascribed to high thermal anomalies.

A three-dimensional (3D) reconstruction of the subsurface of the whole AVGA [16,18–20] was created using data from the intense geothermal exploration drilling and geophysics studies carried out in the area since the 1960s [12]. Based mostly on the geophysical evidence, a granitoid intrusion mingled with mafic magmas located at a depth of about 4 km is supposed to be the heat source for the geothermal system [6,8,21]. Gravimetric models [7,8,22] indicate the presence of a negative NE–SW anomaly centered in correspondence with the volcanic massif and the geothermal fields, interpreted as a low-density body located at shallow crustal levels. Seismic reflection surveys highlight a strong reflector (4–7 km depth), known in the literature as the K-horizon [23–25], whose depth is lower in correspondence with the geothermal fields and the NE outer sector of the volcanic massif. The K-horizon shows an elongated NE–SW shape, whose culmination is centered on the volcanic edifice [22,25] and coincides with the granitoid intrusion (Mt. Amiata magma chamber) and its thermometamorphic contact aureole [6,8,26]. The K-horizon is associated with the 400–450 °C isotherm [24,26]; therefore, it represents the roots of the geothermal systems at depth.

Two water-dominated high-enthalpy geothermal reservoirs are present at increasing depths: i.e., a shallower reservoir hosted in the carbonatic and evaporitic formations of the Tuscan Nappe (with temperatures ranging from 150–230 °C) and a deeper reservoir hosted in a fractured layer of the thermal aureole in the metamorphic basement

where temperatures are higher than 300 °C and up to 350 °C [18,20,27]. The two geothermal reservoirs are separated by low permeability phyllite layers of the regional metamorphic basement [18,20]. Nowadays, only the deeper reservoir is exploited for power generation. Mt. Amiata geothermal reservoirs are both characterized by high gas contents, with CO_2 being the main component (94–95%), followed by CH_4 (1–3.8%) and H_2S (0.5–2.4%) [15,28]. Dome-shaped structures (i.e., gas caps) develop in the shallow reservoir at the contact with the above impermeable formations, where steam and gases produced at depth can accumulate over the liquid phase [18]. These gas caps are composed of 85% gas in the Bagnore geothermal field and 40% gas in the Piancastagnaio field [18], with CO_2 being the most abundant component [28]. The recharge areas in the geothermal system are supposed to correspond with the outcrops of Tuscan Nappe carbonatic formations on a regional scale, where meteoric water can infiltrate at depth [29].

A shallow hydrothermal system is located in the Bagni San Filippo area (characterized by a maximum temperature of 62 °C, S. Filippo 001 exploratory borehole [30]), where the shallow carbonatic and evaporitic reservoir crops out in the Poggio Zoccolino hills, which are one of the recharge areas for the geothermal system. Many thermal spring emergences discharging from this shallow hydrothermal system are present in the Bagni San Filippo area, with temperatures ranging from 42–51 °C, and a Ca–SO_4 composition [14,15,31].

A cold phreatic and potable aquifer with low salinity and a bicarbonate–alkaline composition is hosted in the Mt. Amiata fractured lavas [14,15,32]. The phreatic aquifer is separated from the shallow geothermal reservoir by the presence of impermeable mostly clayey and shaly formations in between, belonging to the Ligurian Units (ophiolites and their pelagic sedimentary cover) and the uppermost clayey formations of the Tuscan Nappe [18,19,32]. More than 150 springs emerging from the volcanic massif and the phreatic aquifer, which is fed by meteoric water and serves numerous towns located in southern Tuscany and northern Latium [19,32,33].

3. Natural Gas Emissions and Origin of CO_2

A recent soil CO_2 flux survey [16] identified a high diffuse natural soil CO_2 flux in the AVGA area reaching 13,275 t/d in a surveyed area of 225 km^2 consisting of 2482 measurement points with a density of 12 stations per km^2. This is the widest and most detailed survey performed in the Italian geothermal areas. In the same paper, high and low soil flux areas were delimited and soil CO_2 degassing was demonstrated to be inhomogeneous, reflecting the geologic structures and geothermal systems related to the volcano feeding system, magma chamber/intrusions, and regional fault systems. Four main high soil flux areas were identified, Bagnore, Piancastagnaio, Bagni San Filippo, and Seggiano. Low and very low soil flux areas were delimited as coinciding with the slopes of the volcanic massif and with the Arcidosso area (see Figure 6 in Sbrana et al. [16]).

Many focused gas emissions are present and are mostly located outside of the volcanic massif. Gases are also discharged by cold springs and Ca–SO_4-rich thermal springs [15,34] and in correspondence with the tunnels and infrastructures of abandoned Hg mines [35–38]. Several papers and databases report the position, chemical, and isotopic composition and flux rates of the gas emissions and thermal and cold springs (i.e., [14,15,35,39]). AVGA gas emissions are composed mainly of CO_2 (85–93% vol.) followed by CH_4, N_2, H_2S, H_2, Ar, CO, and He [14,15]. The tectonic control on gas emissions, thermal springs, travertine deposition, and Hg mineralization in the Pietrineri–Bagni San Filippo area is connected to Quaternary faulting related to the Mt. Amiata and Campiglia d'Orcia transtensional fault systems and the associated releasing step-over zones [40]. Gas leaks are also identified in correspondence with other abandoned Hg mines and are widespread in the Mt. Amiata region, of which the Abbadia San Salvatore mine was the largest and most important one. Hg-rich mineralizations and mines in AVGA are mostly located in correspondence with Quaternary faults and fractures [9,40,41] (Figure 1).

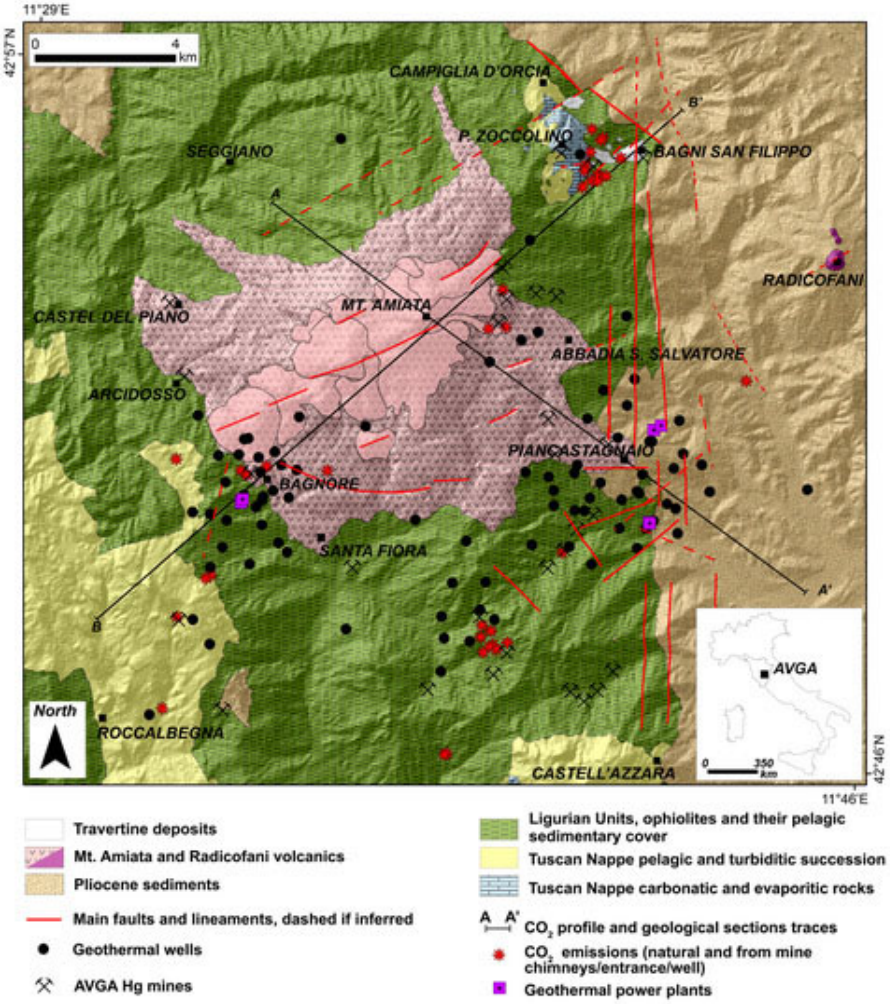

Figure 1. Geological sketch map of the Mt. Amiata volcanic–geothermal area (AVGA) area (modified from [20]).

The origin of CO_2 in the Mt. Amiata region has been discussed and summarized in several papers, where both mantle and crustal origins were hypothesized [14,15,23,42]. The anomalously high CO_2 degassing that affects the peri-Tyrrhenian margin of Italy is mainly related to the degassing of a CO_2-rich mantle based on isotopic and thermodynamic models [31,42]. Mt. Amiata is located inside the Tuscan Roman degassing structure, a belt in which an anomalously high flux of deep CO_2 mainly of mantle origin increases [34]. Consequently, the CO_2 degassing phenomenon is independent of the presence of the geothermal fields, extending over areas larger than those hosting geothermal fields in operation.

However, CO_2 crustal production also derives from thermometamorphic reactions in the deep roots of geothermal fields occurring in the thermometamorphic halos of granitic intrusions, where graphitic phyllites, thermometamorphic carbonates, and marbles are present, furnishing CO_2 of crustal origin [23,27,42–44]. Continuous CO_2 production from the roots of the AVGA system results in constant CO_2 contents over time [42]. A decrease in the CO_2 content of geothermal fluids was recorded only in the early stages of geothermal exploitation in the Mt. Amiata region when the production was limited to the gas caps of the shallow reservoir [18]. In addition to the deeply derived CO_2, CO_2 is also produced in soils by heterotrophic and autotrophic reactions [45].

4. Methods

Soil CO_2 degassing measurements were carried out following the accumulation chamber method described by Chiodini et al. [46]. The employed instrument consists of an accumulation chamber (with a 20 cm diameter) connected to an infrared gas analyzer (LI-8100A LI-COR, Lincoln, Nebraska USA [47]). The infrared analyzer operates in the range of 0–20,000 ppm of CO_2 with an accuracy of 1.5% of reading. The CO_2 flux is computed from the rate of increase of CO_2 concentration in the chamber over time, acquired every 1 s. An exponential regression is fitted to the acquired data to convert the measured concentration to flux values in the LI-COR software.

Measurements were carried out during dry season (June to September) and under stable atmospheric conditions in order to avoid any possible influence of high soil or air humidity.

The dataset of soil CO_2 flux measurements (Table S1) was afterward elaborated with statistical methods, applying the graphical statistical approach (GSA) method described by Chiodini et al. [46]. The log-normal probability plot is widely used to identify geochemical log-normal populations [48]. Data plotting as a straight line on the log-normal probability plot is characterized by a single population, while two or more populations plot as a curve, identified by n−1 inflection points. Log-normal populations in geothermal and volcanic areas are usually represented by a polymodal distribution, with a low soil flux population representing the biological activity of the soil, typically referred to as the background, and by a high soil flux population representing the hydrothermal or magmatic contribution; therefore, the CO_2 generated at depth [49] is typically called an anomalous flux. The Sichel's *t* estimator [50] was used to calculate the mean flux, standard deviation, 95% confidence interval, and threshold of the identified log-normal populations.

The sequential Gaussian simulation (sGs) technique [49] was used to compute the soil CO_2 flux maps and the total CO_2 release from diffuse degassing from the soil. The sGs technique is widely used and preferred in the most recent soil CO_2 flux literature over other techniques (e.g., GSA in Chiodini et al. [46]) and over other mapping and interpolation techniques (e.g., the Kriging algorithm). In particular, in the GSA technique, threshold choice is greatly arbitrary and the spatial distribution of data is not considered. In contrast, even if the Kriging algorithm is a spatial interpolation technique that contemplates the spatial distribution of data, it does not honor the statistical distribution of the experimental dataset. The sGs is a stochastic simulation algorithm that considers both the spatial correlation and the statistical distribution of the experimental data and allows for the quantification of the uncertainty estimated over a simulation grid from 100 equally probable realizations [49]. Stanford Geostatistical Modeling Software [51] was used to perform the geostatistical elaboration of the collected soil CO_2 flux measurements, run the sGs algorithm, and post-process the results. The total soil CO_2 degassing was computed as the sum of the product of simulated values of each cell in the simulation grid by the value of the simulation grid area [49].

5. Results

A new soil CO_2 flux survey was performed in the Mt. Amiata area in the summer of 2019 to expand the previously investigated area and delimit the degassing areas. Starting from the previously surveyed area, the new soil CO_2 flux survey was extended toward the south and south-east, now completely covering Bagnore and Piancastagnaio geothermal fields and a portion of the Paglia River Valley. There were 738 new soil CO_2 flux measurements collected over an area of about 60 km^2. The survey was performed using the same technique defined in the previous work with the same instrument under dry and stable weather conditions. The measurements were collected over a regular grid with a spacing of 250 m to maintain consistency with the previous general survey and integrate all data. Sbrana et al. [16] concluded that the selected grid spacing was the best

choice for a regional survey like this, considering the wide area under investigation, and showed that the grid spacing used was sufficiently accurate and adequate to reveal and highlight the main degassing areas and structures, although small-scale degassing structures were not detected. The southeastern sector of the new survey, characterized by the presence of cultivated fields and pastures, was successfully covered with a regular grid of soil CO_2 flux measurements, while the presence of steep and impervious morphology prevented covering the southern part of the surveyed area with an equally spaced grid of soil CO_2 flux measurements (Figure 2).

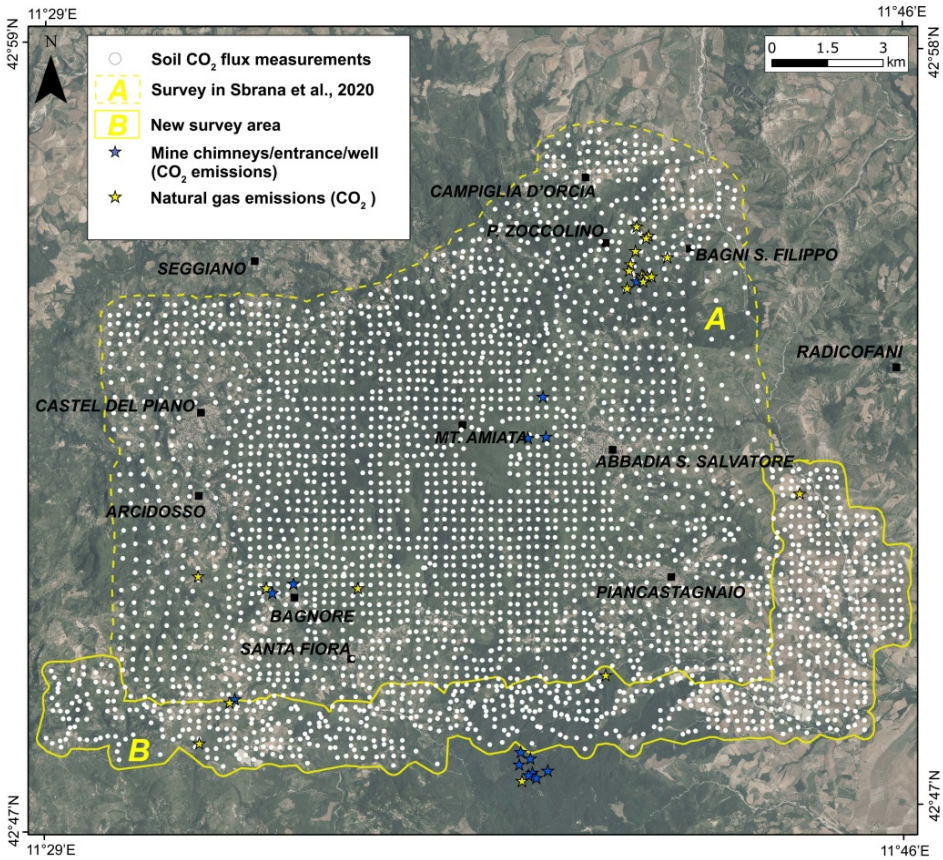

Figure 2. Measurement points for the first A and second B surveys.

Because this work aims to estimate the total soil CO_2 flux over the Mt. Amiata area and that the two surveys were both made during the summer season under the same weather conditions, the whole soil CO_2 flux dataset was treated as a single dataset comprising 3208 measurements spanning over an area of 280 km^2 with a coverage of about 12 measures per km^2. A few measurements were discarded from the analytical treatment when the regression coefficient (R^2) of the exponential regression of the fitting curve to the measured concentration in the chamber within the time exceeded 0.85.

Soil CO_2 flux values in the Mt. Amiata area range from 0.43 up to 296.41 μmol m^{-2} s^{-1} (1.6–1127 g m^{-2} d^{-1}) (Table 1 and Figure 3).

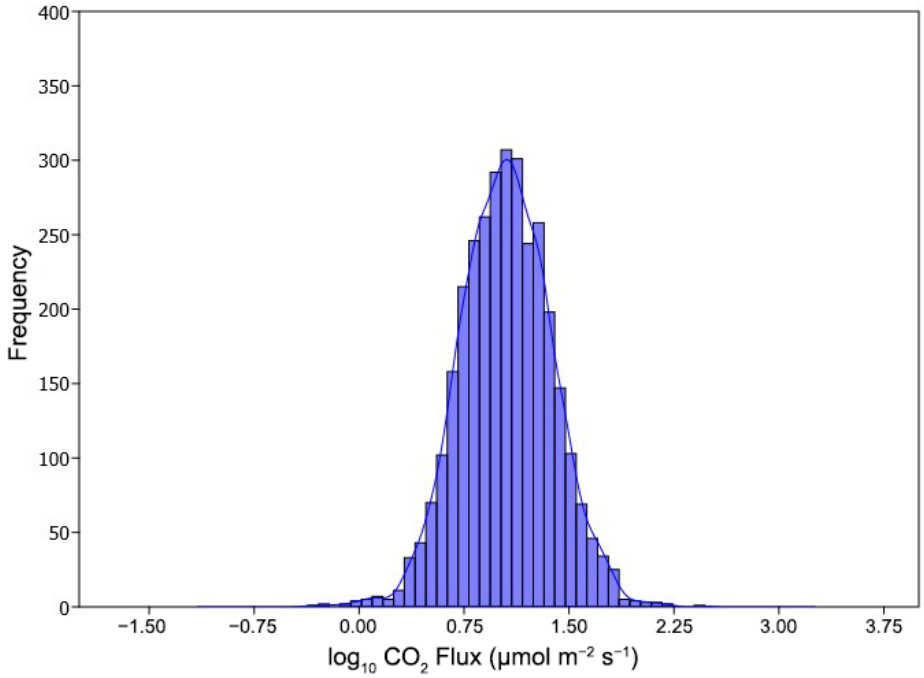

Figure 3. Frequency plot of soil CO_2 flux measurements. Range from 0.43 up to 296.41 μmol m^{-2} s^{-1} corresponds to −0.37 to 2.47 $\log_{10}$ CO_2 flux values.

The dataset was analyzed through the GSA method, and data were plotted on the log-normal probability plot [49]. Even though the log-normal probability plot of soil CO_2 flux data in the Mt. Amiata area (Figure 4) does not show a clear polymodal statistical distribution, the partitioning of the flux data was performed as described by Sinclair [48] and Chiodini et al. [46]. Two inflection points were observed that identify three overlapping log-normal populations: i.e., population A (inflection point at 0.77 $\log_{10}CO_2$, μmol m^{-2} s^{-1}), population C (inflection point at 1.55 $\log_{10}CO_2$, μmol m^{-2} s^{-1}), and a third population (population B) made up of a mixture of populations A and C.

Table 1. Summary statistics of the entire soil CO_2 flux dataset in the Mt. Amiata region.

Surveyed Area (km^2)	Number of Measurements	CO_2 Flux Range (μmol m^{-2} s^{-1}) (g m^{-2} d^{-1})	CO_2 Flux Mean (μmol m^{-2} s^{-1}) (g m^{-2} d^{-1})	CO_2 Flux Median (μmol m^{-2} s^{-1}) (g m^{-2} d^{-1})
280	3208	0.43–296.41 (1.6–1127)	14.97 (56.9)	11.2 (42.6)

The summary statistics for populations A, B, and C are shown in Table 2. Sichel's *t* estimator [50] was used to calculate the mean flux, standard deviation, 95% confidence interval, and threshold of the log-normal populations identified with the procedure proposed by Sinclair [48]. Population A is defined by a mean of 4.9 μmol m^{-2} s^{-1} (18.6 g m^{-2} d^{-1}) and a threshold of 10.41 μmol m^{-2} s^{-1} (39.6 g m^{-2} d^{-1}) and represents 20% of the dataset. Population A denotes the pure biological background population. Population C represents 6% of the dataset and is defined by a mean of 49.75 μmol m^{-2} s^{-1} (189.2 g m^{-2} d^{-1}) and a threshold of 32.6 μmol m^{-2} s^{-1} (123.9 g m^{-2} d^{-1}). Population C is the pure hydrothermal population characterized by high CO_2 fluxes. Finally, 74% of the dataset (population B) is represented by a mixture of populations A and C. No data about the ^{13}C isotopic content of soil CO_2 are available; thus, the partitioned populations cannot be addressed equivocally to the biological background or to the deep hydrothermal production.

Table 2. Summary statistics of the partitioned populations.

CO_2 Population	Proportion (%)	Mean and 95% Confidence Interval (μmol m^{-2} s^{-1}) (g m^{-2} d^{-1})	Threshold (μmol m^{-2} s^{-1}) (g m^{-2} d^{-1})
Population A	20	4.9 (4.78–5.03) [18.6 (18.18–19.13)]	10.41 (39.6)
Population B	74	12.3 (12–12.6) [46.8 (45.6–48)]	25 (95)
Population C	6	49.75 (47.6–51.7) [189.2 (181–196.6)]	32.6 (123.9)

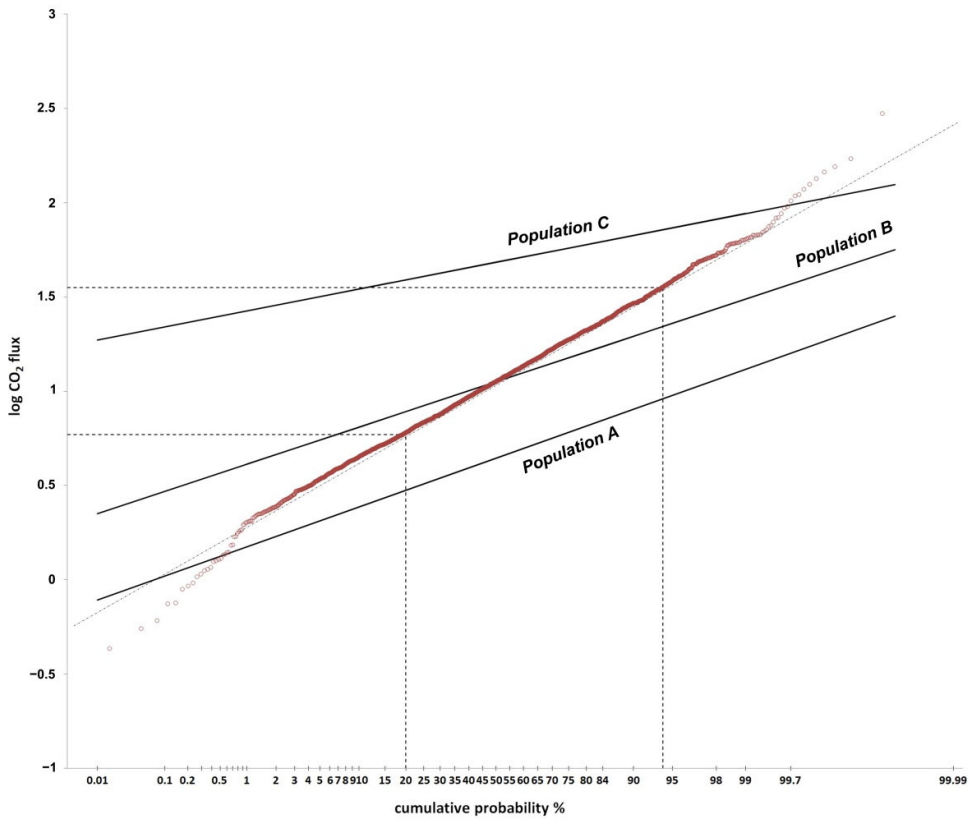

Figure 4. Log-normal probability plot of soil CO_2 flux measurements. The partitioned populations [48] and the inflection points are shown. A dashed straight line traced through the central part of the plot helps visualize the chosen inflection points.

6. Discussion

6.1. Natural CO_2 Flux

The whole dataset of 3208 measurements available for the Mt. Amiata region was used to compute the soil CO_2 flux maps and the total CO_2 release from diffuse soil degassing using the sGs technique [49]. There were 100 equiprobable realizations of the soil CO_2 flux produced over a 50 · 50 m simulation grid. The resulting map of Mt. Amiata soil CO_2 flux, representing the average of the 100 realizations is presented in Figure 5.

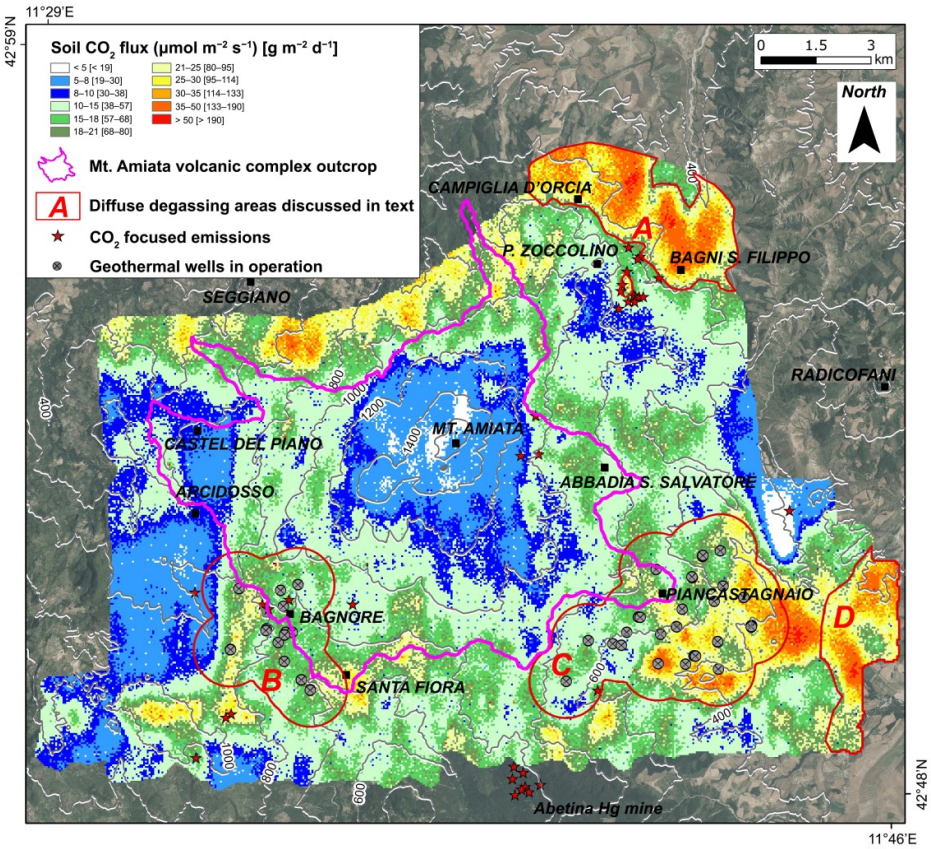

Figure 5. Soil CO_2 flux map with areas of Bagnore, Piancastagnaio (geothermal fields in operation, brownfields), Bagni San Filippo (geothermal greenfield), and Paglia River high emission areas. Red stars are the concentrated gas emissions and gas vents considered in the CO_2 total emissions budget in the atmosphere. The geothermal wells in operation used to define B and C areas are also reported (Enel Green Power data).

The highest slopes of the volcanic massif (with the highest peak of 1730 m) are characterized by low CO_2 flux values near the biological background (Figure 5). Similar low soil CO_2 flux values are also found in a broad area in the western sector of the area. The lowest slopes of the volcanic edifice are instead characterized by soil CO_2 flux values higher than the biological background threshold (10.41 μmol m^{-2} s^{-1} or 39.6 g m^{-2} d^{-1}). High soil CO_2 flux anomalies (higher than the background threshold) characterize the geothermal fields of Bagnore (B area) and Piancastagnaio (C area), where steam and gases accumulate in a dome-shaped structure (i.e., gas caps) present at the top of the shallow carbonatic–evaporitic geothermal reservoir. These geothermal areas are delimited using the influence radius in reservoirs of the geothermal deep production wells. Other important high soil CO_2 fluxes are found in the Bagni San Filippo area and in the river Paglia valley. These greenfield and high emission areas are delimited by the 20 μmol m^{-2} s^{-1} isoflux line on the sGs map. In the Bagni San Filippo area, the highest soil CO_2 fluxes are recorded in correspondence with the western border of the Radicofani basin and its master faults system, and in the Inferno area, CO_2-focused emissions are also present and in correspondence with the Campiglia d'Orcia NE–SW fault system (north of the volcanic massif). A structural control on the Paglia River Valley is inferred by looking at Figure 1, where buried normal faults related to the graben structure could have driven the NW–SE valley incision.

In the AVGA, high soil CO_2 fluxes are found in correspondence with the infrastructures, tunnels, and mine shafts of Hg mines, where Quaternary faults and fractures

are widespread, in correspondence with the Pietrineri, Bagnore, Mt. Labro, and Senna Morta mining areas (the latter is located between Piancastagnaio and Poggio Nibbio) (Figure 1).

Using the background threshold (Table 2) as the cutoff value, the probability that soil CO_2 flux exceeds this value highlights the diffuse degassing structures [49]. The probability map (Figure 6) emphasizes areas where the biological background prevails in addition to areas of diffuse anomalous degassing (deep carbon populations B and C), highlighting the strong soil CO_2 diffuse degassing that affects the whole Mt. Amiata volcano geothermal area, with many areas showing anomalous fluxes.

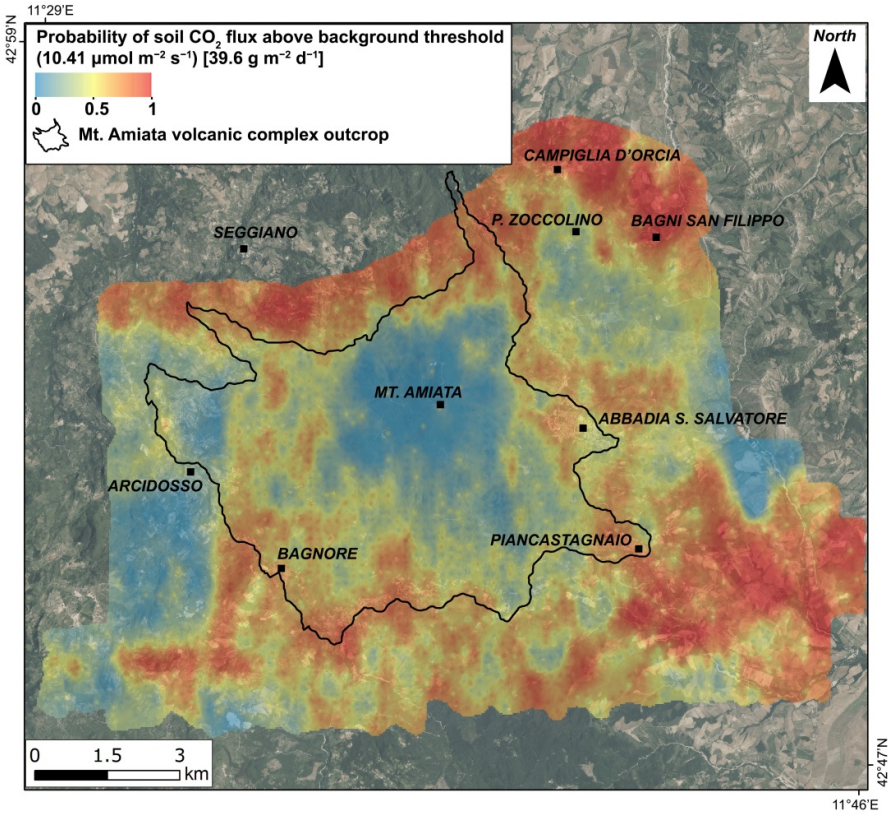

Figure 6. Probability map of occurrence of soil CO_2 flux higher than the background threshold.

The total soil CO_2 degassing over the whole Mt. Amiata area and its uncertainty was calculated with the sGs technique. The total natural CO_2 output, computed as the sum of the product of simulated values of each cell in the simulation grid by the value of the simulation grid area, represents the average of the 100 equiprobable realizations. The total natural soil CO_2 degassing was estimated as 16,254 t/d, with a 95% confidence interval of 15,800–16,642 t/d. The biological contribution was estimated as 5,217 t/d and the deep contribution was estimated as 11,037 t/d based on the mean of the partitioned populations A and C.

Given the survey area of 280 km^2, a mean emission rate of 58 t/d km^2 was estimated based on the total natural soil CO_2 output. An emission rate of 115 t/d km^2 was estimated for the Bagni San Filippo high soil CO_2 flux area (A in Figure 5), while emission rates ranging from 154–200 t/d km^2 [15,35,36] were estimated from localized high soil CO_2 degassing areas only. The lower emission soil CO_2 flux area coincides with the upper slopes of the volcanic edifice, characterized by the presence of a climate forested zone, where an emission rate of 27 t/d km^2 was computed [16]. Sbrana et al. [16] explained this very low soil flux on the dome complex volcano as being due to the lamination of the

shallow geothermal reservoir to the presence of a phreatic aquifer grading upward in thick water unsaturated fractured lavas of the dome complex. In this framework, the increase of deep CO_2 appears to be slowed down. For more details on the subsoil geology of AVGA, see the paper by Sbrana et al. [16], which reports a reconstruction of the buried structures.

Soil CO_2 flux profiles in relation to simplified geological sections help to visualize the main degassing structures. In Figures 6 and 7a, the geochemically anomalous soil CO_2 flux areas (where fluxes are higher than the background threshold, 10.4 μmol m^{-2} s^{-1}) of Piancastagnaio and Bagnore geothermal fields are well evidenced south of the volcano. These wide degassing areas span from about 25 km^2 for Bagnore and about 35 km^2 for Piancastagnaio. These two areas were computed considering only the geothermal wells in operation (Enel Green Power data) as the surface projection of the interference area of the wells in the geothermal reservoir. In the northern AVGA, high emission areas are delimited. The most intense and wide are the greenfield areas of Bagni San Filippo and Seggiano.

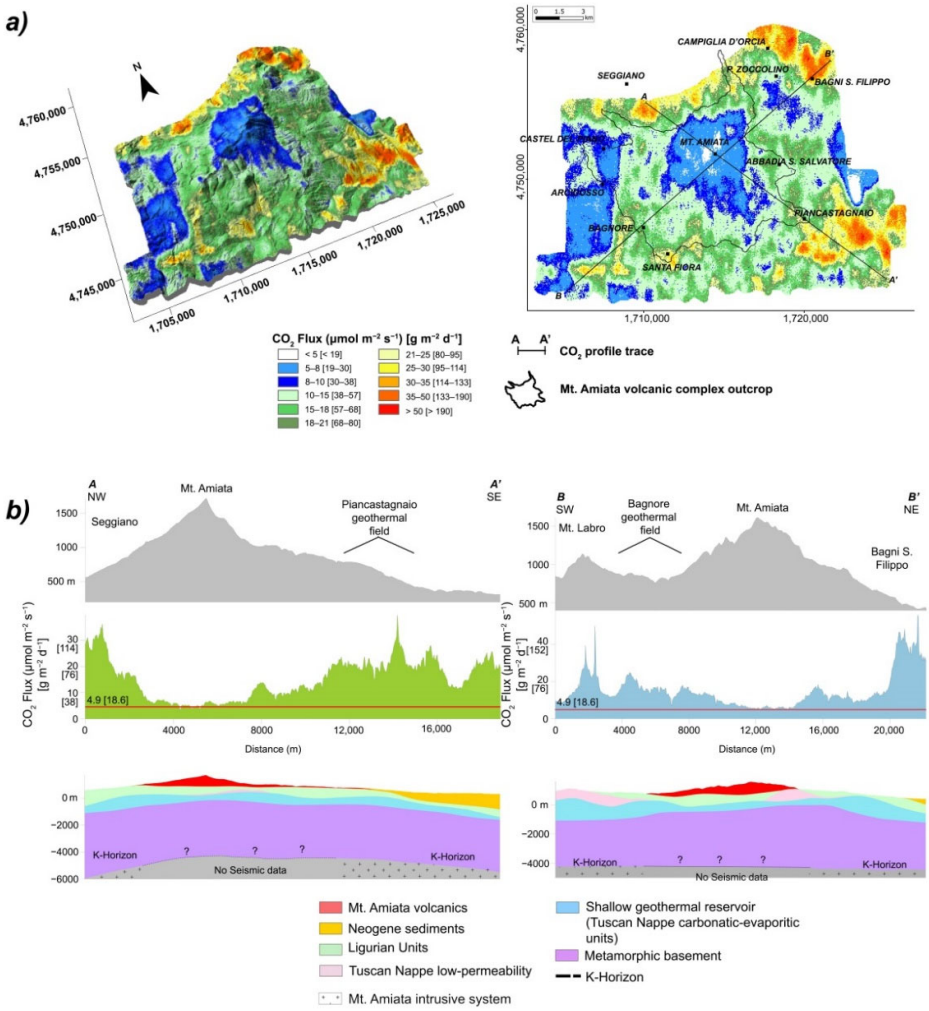

Figure 7. (**a**) sGs map of soil CO_2 flux AVGA superimposed on a 3D DTM (Digital Terrain Model) of AVGA; (**b**) Soil CO_2 flux profiles in relation to topographic profiles and geological sections reporting the main geological formations and the K-horizon, proxy of the granite intrusion.

The soil flux profiles (Figure 7b) describe the degassing areas well. In profile AA', the maximum gas flow rate occurs in the Piancastagnaio field, reflecting the presence of the relatively shallow and thick carbonatic–evaporitic reservoir. At the top of this reservoir, a CO_2 vapor gas cap in the upflow zone of a robust convection system has developed. Furthermore, the K-horizon is relatively shallow at a depth of approximately 4.5 km. The K-horizon is the proxy of the granitic intrusion. In the thermometamorphic aureole of granites, CO_2 is produced by thermometamorphic reactions feeding the geothermal reservoirs, and finally, the diffuse soil degassing is observed. In the same profile, an area of anomalous flux was observed in the Seggiano area.

In profile BB', an increase of flux between 15 to 20 μmol m^{-2} s^{-1} was shown in correspondence with the Bagnore field, while the strongest values occur in the greenfield areas of Bagni San Filippo and Mt. Labro.

6.2. CO_2 Emissions from GPPs

The effect of geothermal power production on natural surface manifestations is still little known. Bertani and Thain [52] have shown that geothermal power production led to a decrease in surface CO_2 natural manifestations in the Larderello geothermal field (Italy). Frondini et al. [15] suggested that surface manifestations in the Mt. Amiata geothermal field could have also decreased because of geothermal energy exploitation; however, predevelopment CO_2 emissions in the Mt. Amiata region are not available. Bertani and Thain [52] suggested that if the reduced natural manifestations are countable, they should be subtracted from the GPP emissions. In some other foreign geothermal fields, however, CO_2 surface emissions have increased in response to the exploitation and to the reduced reservoir pressure, e.g., as observed in the Reykjanes geothermal field in Iceland [53,54]. It is important to notice that AVGA and Iceland are characterized by very different geological contexts. Observation data relative to the Icelandic soil CO_2 flux are furthermore not areal normalized, which makes comparing the greenfield and brownfield areas more difficult.

In the Mt. Amiata region, six GPPs are distributed between the Bagnore and Piancastagnaio geothermal fields, with a total installed capacity of 121 MW (Table 3). Three GPPs, two single flash units, and a binary group (ORC, Organic Rankine Cycle) are located in the Bagnore geothermal field, while three single flash units are located in the Piancastagnaio geothermal field (Figure 1). The annual electricity production in the Mt. Amiata region in 2018 was 1070.8 GWh [55], which represented 18% of the total geothermal electricity production in Italy (6105 GWh) [56].

Table 3. Geothermal power plants (GPPs) in the Mt. Amiata region [13].

Plant Name	Year Commissioned	Number of Units	Type	Installed Capacity (MWe)
Bagnore 3	1998	1	Single Flash	20
Binary Group Bagnore3	2013	1	Binary-ORC	1
Bagnore 4	2014	2	Single Flash	40
Piancastagnaio 3	1990	1	Single Flash	20
Piancastagnaio 4	1991	1	Single Flash	20
Piancastagnaio 5	1994	1	Single Flash	20
Total	-	-	-	121

The CO_2 emissions data from Italian GPPs are published annually by the Tuscany Regional Agency for Environmental Protection [13,57,58]. CO_2 represents the most abundant noncondensable gas emitted from Mt. Amiata GPPs, corresponding to 95.6% of the gas phase [28]. In addition, CO, H_2S, NH_3, CH_4, Hg, As, Sb, N_2, He, Ar, and Se constitute the gas phase of the geothermal fluids in the Mt. Amiata reservoir [13,15,28].

Table 4 shows the CO_2 emission values from the single flash power plants in the Mt. Amiata area. In 2018, a CO_2 emission factor of 484 g/kWh was calculated as an average of

all Mt. Amiata GPPs, while the emission factor computed for 2016 was 524 g/kWh (Piancastagnaio 5 data are missing) and for 2014 was 503 g/kWh (Bagnore 4 data are not considered). Bravi and Basosi [59] reported a weighted averaged emission rate of 497 g/kWh from 2002 to 2009. The total CO_2 emissions from GPPs in the Mt. Amiata area were 515,193 tons in 2018.

Table 4. Mt. Amiata GPPs' CO_2 emissions. Number of GPPs sampled by ARPAT compared to the total installed. Total CO_2 emissions from GPPs are computed after ARPAT inventories [13,58]; 2016 data are after [57] and [60]. Annual electricity production for Mt. Amiata GPPs data after: (a) [55]; (b) [60]; (c) [61]. (d) CO_2 emission factor years 2002–2009 after [59].

Year	No. of GPPs	GPPs' Total Annual CO_2 Emissions (t/y)	Annual Electricity Production (GWh/y)	CO_2 g/kWh
2018	5/5	515,193	1064 (a)	484
2016	4/5	449,299	842 (b)	524
2014	4/4	342,669	681 (c)	503
2002–2009	Variable	-	-	497 (d)

The emission factors from GPPs around the world are shown in Table 5 for comparison. The CO_2 emissions from GPPs in the Mt. Amiata area are rather high if compared to the global world weighted average of 122 g/kWh [52] and the emissions of other GPPs around the world (except for Turkey and Larderello, Italy), but they are still small compared to emissions from traditional thermal power plants (Table 6). The CO_2 emissions for electricity generation from fossil-fueled power plants in Italy from 2017 [62] are reported in Table 6. Fossil-fueled power plants accounted for 70.5% of the total annual electricity generation in 2017. Table 7 shows that CO_2 emissions from Mt. Amiata GPPs are lower than thermal fossil-fueled power plants, except for natural gas power plants. The emissions from coal power plants are about two times greater than that of GPPs and the derived gas emissions are three times greater.

Table 5. CO_2 emission factors from GPPs around the world.

Geothermal Area	Year	CO_2 g/kWh	Reference
Larderello (Italy)	2018	343	Calculated based on ARPAT data
Italian geothermal fields (average)	2014	321	[63]
Italian geothermal fields (average)	2015	343	[63]
Italian geothermal fields (average)	2016	311	[63]
Iceland	2018	26	[64]
Iceland	2012	34	[65]
Indonesia	2013	62.9	[66]
USA	2003	91	[67]
USA	2010	25.7	[68]
California	2014	107	[65]
California, the geysers	2013	45	[65]
California, Coso	2013	245	[65]
New Zealand	2012	104	[65]
Turkey	2014	1050	[65]
Global	2001	122	[52]

Table 6. CO_2 emission factors from fossil-fueled power plants in Italy [62].

Fossil-Fueled Power Plants	CO_2 g/kWh (2017)	Percentage of Fossil-Fuel Electricity Production in 2017
Coal	870	15.6
Natural gas	368.3	67.2
Derived gas	1498.4	1.2
Petroleum	548.9	5.5
Others *	133.3	10.5

* other solid and gaseous fuels including biomethane.

6.3. Merging Natural Soil CO_2 Flux and GPPs' CO_2 Emissions

The different components comprising the CO_2 budget for emissions in the AVGA are in the order of abundance: soil diffuse emissions, GPPs, and focused emissions (gas vents, thermal pools, and Hg mine infrastructures). All of the total collected data reported in Table 7 are visualized in the bar diagram shown in Figure 8, where the different single components and their sum are illustrated. The total soil CO_2 flux is subdivided into the background flux values (calculated by means of data statistics) coinciding with the biological population A of Figure 4 and in the deep CO_2 populations B and C of Figure 4 coinciding with the CO_2 naturally formed in thermometamorphic aureole of the volcano magma chamber intrusion and rising from deeper magmatic mantle sources. The total CO_2 emitted in the AVGA is estimated as 17,934 t/d (as shown by the right bar of Figure 8), of which diffuse deep CO_2 is 11,038 t/d, where the 262 t/d of focused emissions must be added to this value. The total deep CO_2 reaches 11,300 t/d. The CO_2 emissions of the six GPPs of Bagnore and Piancastagnaio fields sum to 1418 t/d, which represents 7.9% of the CO_2 emitted in the atmosphere in the AVGA.

Table 7. CO_2 soil fluxes in different areas (brown and greenfields). GPPs data from [13]. (*) Sum of all CO_2 focused emissions in the Mt. Amiata volcanic–geothermal area (AVGA) area.

Diffuse Degassing Area	Diffuse CO_2 Degassing (Biological Component) (t/d)	Diffuse CO_2 Degassing (Deep Component) (t/d)	GPPs (t/d)	CO_2 Focused Emissions (t/d)	Sum (t/d)
Piancastagnaio (24.8 km^2) (brownfield)	463	1466	770	-	2699
Bagnore (14.5 km^2) (brownfield)	270	635	648	2	1555
Bagni San Filippo (12.3 km^2) (greenfield)	229	1186	-	144	1559
Paglia Valley (7.13 km^2) (greenfield)	133	599	-	-	732
Survey Area (280 km^2)	5216	11,038	1418	262 (*)	17,934

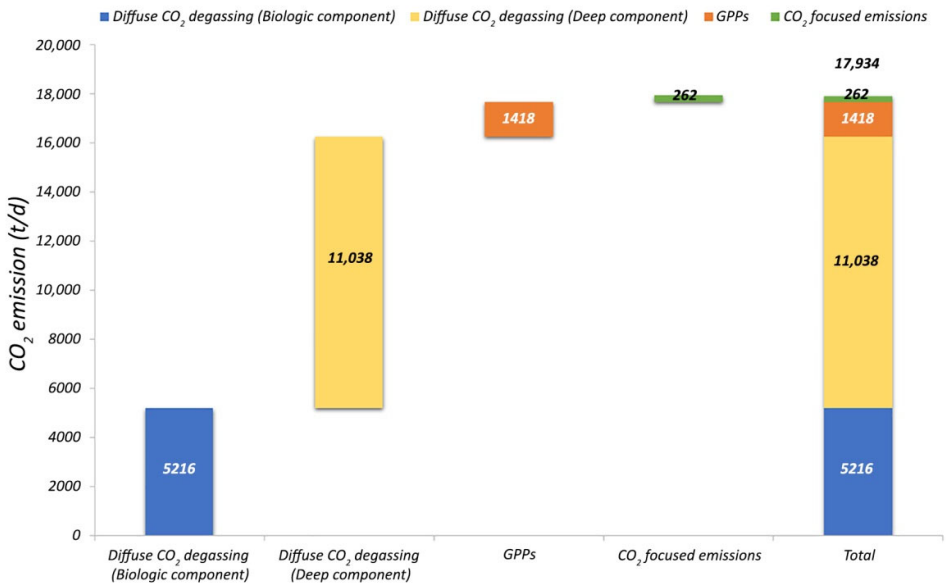

Figure 8. Total CO_2 emissions in AVGA, split in its components.

Another important focus concerns the analysis of the high CO_2 flux areas. As previously stated, these areas coincide with the Bagnore (area B in Figure 5) and Piancastagnaio (area C in Figure 5) geothermal fields and with the greenfield areas unaffected by geothermal operations of Bagni San Filippo (area A in Figure 5) and Paglia (area D in Figure 5). Figure 9 shows the emissions in the different high soil flux areas expressed as t/d. Similar emissions are observed in different areas and separated into the background (biological), deep, GPPs' emissions, and focused emissions. Because of the different areal extent of the high emission areas, a better way to analyze data is to normalize emissions for areas expressed as t/d km^2.

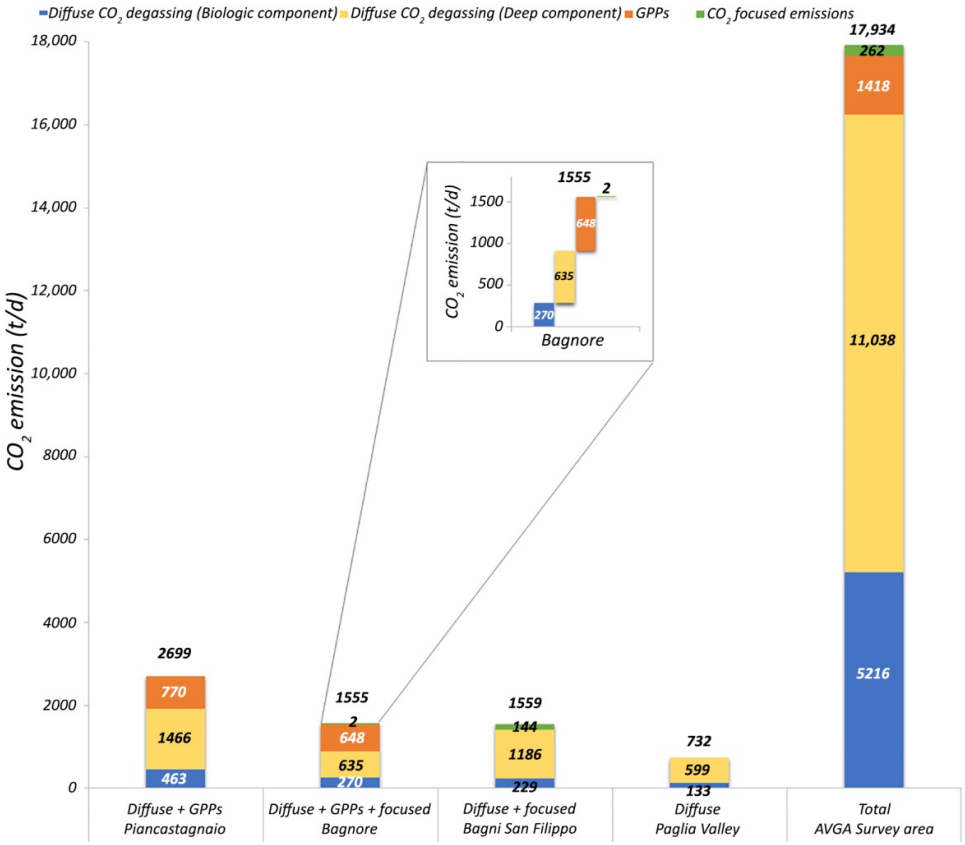

Figure 9. CO_2 emissions in the four high emission areas and in the AVGA area. In the Bagnore and Bagni San Filippo areas, only CO_2-focused emissions located inside the two identified areas are considered.

Figure 10 highlights first that a very similar normalized emission occurs ranging from 103–115 t/d km^2 in the four areas. These data point to the general observation that the CO_2 flux from deep sources is homogeneous in the AVGA. This observed behavior is most probably linked to the mechanisms of natural generation of CO_2 that several researchers [16] claim are because of the thermal processes in the thermometamorphic contact aureole of the Mt. Amiata volcano shallow magmatic systems and to the deeper mantle-generated and -released CO_2. The large volumes of the relatively shallow (4–5 km depth) magmatic system extending in subsoil over the whole AVGA allow for the homogeneous release of CO_2 in particular in correspondence with the vertical projection of the shallower portions of the magmatic system. The homogeneous emission of gas allows us to compare the gas flux between the areas where natural emissions are undisturbed and the areas where the production of electricity is active. The consequence of the collection, processing, and analysis of the presented data is that if the homogeneous deep gas flow is established over large areas, then the undisturbed areas can be taken as a reference to the medium-deep natural flow by verifying the effects of electricity production activities on the natural flux of gas in geothermal fields.

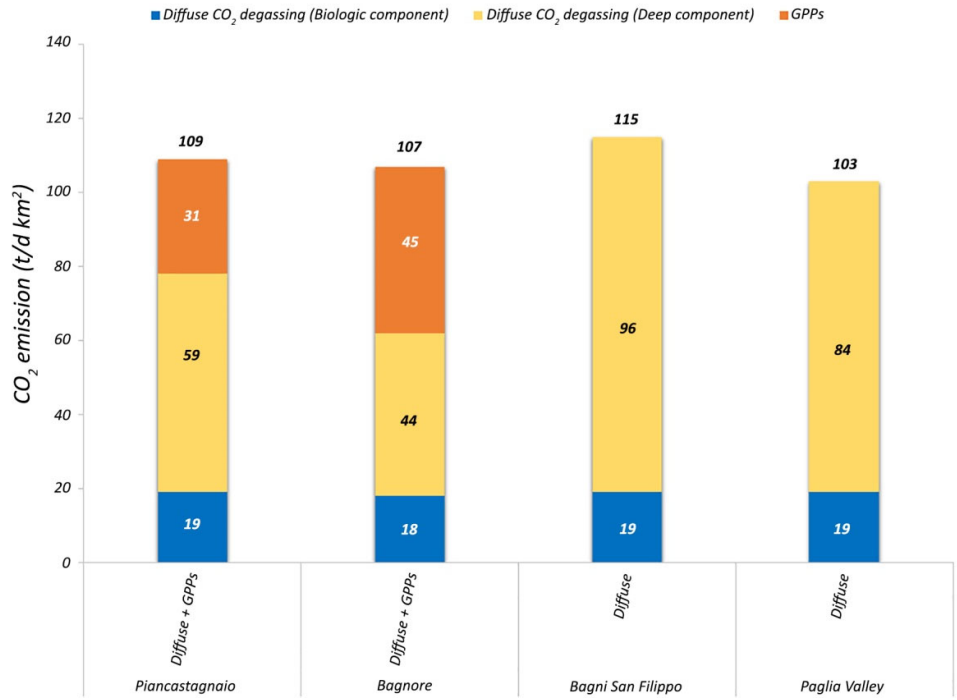

Figure 10. Comparison of the areal normalized CO_2 emissions from different sources (biological, deep, geothermal power plants (GPPs)) in the high emission areas of AVGA, greenfields, and brownfields. The contribution of CO_2 focused emissions have been neglected because of their very slow relative contribution.

Figure 10 also shows another key point for this study's objectives. The natural emissions measured from soils are considerably lower in areas of the geothermal fields (Figure 10 and Table 8). For the Bagnore area, the contribution of deep CO_2 to the diffuse soil flux to the atmosphere is the same as that of emissions from power plants. For the Piancastagnaio area, the contribution to diffuse emissions of deep CO_2 is double that of CO_2 emissions from power plants. However, summing up the total emissions from soils plus the emissions from the GPPs, we observe that the emissions in geothermal areas are the same as those occurring in greenfield areas.

Table 8. Areal normalized natural and GPPs CO_2 fluxes, greenfields, and brownfields. GPPs calculated based on data from [13].

Diffuse Degassing Area	Diffuse CO_2 Degassing (Biological Component) (t/d km^2)	Diffuse CO_2 Degassing (Deep Component) (t/d km^2)	GPPs (t/d km^2)	Sum (t/d km^2)
Piancastagnaio (24.8 km^2) (brownfield)	19	59	31	109
Bagnore (14.5 km^2) (brownfield)	18	44	45	107
Bagni San Filippo (12.3 km^2) (greenfield)	19	96	-	115
Paglia Valley (7.13 km^2) (greenfield)	19	84	-	103

We can observe that the Bagnore and Piancastagnaio soil emissions are significantly smaller if compared to Bagni San Filippo and Paglia areas, but they become equivalent if the contribution of GPPs emission is included in the flux. This finding shows that the

depletion of emissions in the developed geothermal area is nearly balanced by the contribution of GPPs.

6.4. The Conceptual Model

All data collected, elaborated, and analyzed may be resumed in a conceptual model for CO_2 degassing in the AVGA and may be useful in better defining the implications of the interplay of processes of natural degassing and the effects of the superposition of electricity production. Figure 11 shows a 3D sketch of the Piancastagnaio geothermal field and the Bagni San Filippo greenfield geothermal system, which can be used to easily visualize the observed processes of formation, transport, and release on the surface of the Earth in the AVGA.

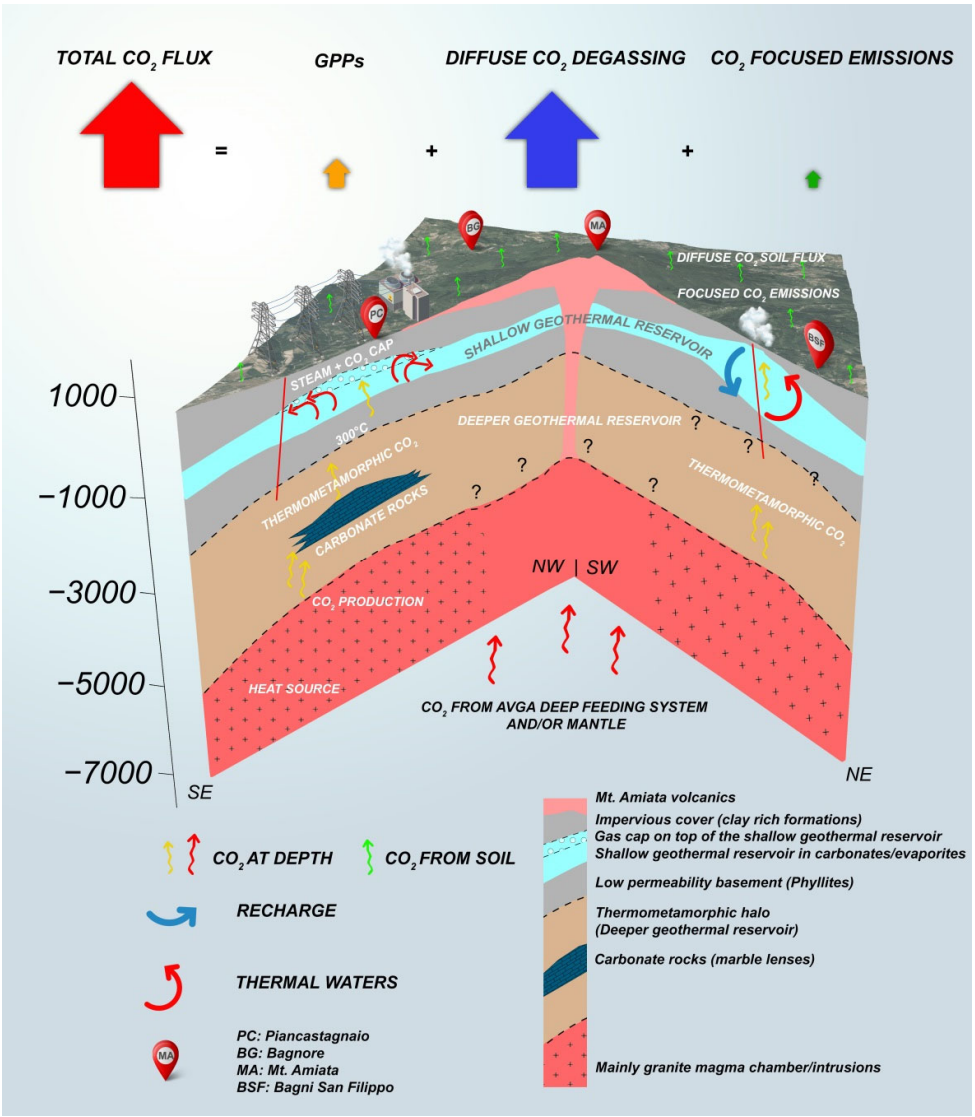

Figure 11. Conceptual model exemplified in a section crossing the Piancastagnaio geothermal field and the undisturbed Bagni San Filippo area (Icons designed by macrovector/Freepik).

Our data suggest that from a statistical point of view, CO_2 is mainly of deep origin with a contribution because of the biological activity of soils and plants. Deep CO_2 derives by the contribution of the mantle, deep magmatic systems and by the thermometamorphic processes acting at shallow depths at the interface between granites and its

wall rocks where thick layers of cornubianites form. The granite depth is revealed by the K-horizon reflector (the deep roots of the AVGA geothermal system). The CO_2 from this source is preferentially transported upwards by the convective systems developed inside the water-dominated deep fractured geothermal reservoir hosted in thermometamorphic phyllites. From this geothermal deep reservoir, gases rise upward to feed the shallow geothermal reservoir hosted in porous fractured carbonatic–evaporitic rocks. The convection of the high temperature, aqueous fluids in reservoirs, and tectonic traps induce the formation of NCG (non-condensable gases) gas and vapor accumulations at the reservoir top because of the permeability contrast with the overlying clay-rich impermeable cover formation. The impermeable cover of geothermal systems stops rising up of the aqueous fluid, but it is not impermeable to gas, thus allowing the gas to rise to the surface and fueling the widespread CO_2 diffuse emissions that characterize this area. In the presence of tectonic breaks (faults and fractures) in impermeable subsoil formations or the absence of impermeable formations at the top of geothermal reservoirs, concentrated gas emissions, i.e., gas vents, occur.

The analysis of the natural CO_2 flux from soil and concentrated emissions (gas vents, active fault systems, mining areas, and GPPs' emissions) highlights that a total CO_2 emission of 17,934 t/d occurs in the AVGA. The comparison with the emissions from the GPPs (1418 t/d) show that only 7.9% of the total carbon flux was issued by GPPs. Consequently, the performed survey for this whole geothermal area of Italy can define the true ratio between the natural emissions from the crust to the atmosphere occurring in this area and the emissions measured in GPPs. We demonstrate first the low contribution of geothermal energy production to increase the contribution of CO_2 emissions to the atmosphere. In general, this represents the first important improvement of the existing knowledge about the GPPs' CO_2 emissions and demonstrates the importance of defining the natural emissions in the geothermal areas for a better understanding of the true role of GPPs in greenhouse gas emissions. This topic is further discussed in the following points.

Four diffuse high emission areas with very high values of natural gas fluxes from the soil were discovered and areal bounded. These areas mainly coincide with AVGA geothermal/hydrothermal systems in which convective processes are strongly active. The CO_2 that forms in the thermometamorphic aureole of the magma chamber/intrusions of the Mt. Amiata volcano, in the deeper portions of the magmatic system, and rising from the mantle is preferentially transported upward in water-dominated geothermal convection cells formed in the shallow and deep geothermal reservoirs. Data analysis for these four areas shows that the global CO_2 flux, natural plus power plants flux, is similar between the areas. The CO_2 flux stands at 103–115 t/d km^2.

Two of the areas coincide with the upflow areas of the Bagnore and Piancastagnaio geothermal fields and have been in operation for 60 years (brownfields), while two areas are located in areas not in operation for geothermal production (greenfields). The highest emissions are observed in the Bagni San Filippo area and are diffuse and concentrated (in faults, water thermal pools natural manifestations, gas vents, and in correspondence with disused Hg mining sites) and in the Paglia River area. The comparison between the geothermal and the latter areas highlights that the total flow (t/d km^2) is practically coinciding around a mean value of 110 t/d km^2, if the GPPs emission is included in the budget, while the diffuse natural flow in geothermal areas is much lower. In the Bagnore area, it slightly exceeds 55% of the total flow, while it is higher than 70% of the total flow in Piancastagnaio.

These experimental data indicate very high gas soil diffuse and concentrate emissions in the AVGA, which are relatively constant in the various sectors of the volcanic geothermal district. This is possibly because of the occurrence of a relatively homogeneous process of CO_2 generation at depth over a roughly circular area mainly coinciding with the deep roots of the AVGA feeding system (magma chamber/intrusions and related thermometamorphic halo and more in the general volcano plumbing system).

In this framework, in the areas of geothermal fields, the survey shows that the diffuse natural emissions of gas markedly decrease. If we add the emissions from the area of power plants (calculated on the reservoir area in operation) to the soil diffuse emissions of the same area, a good match is observed with those of the undisturbed (greenfield) areas of Bagni San Filippo and Paglia. These data indicate that the gas emissions linked to the operation of power plants substantially balances the natural gas soil flux that appears markedly reduced in operation areas. The values of CO_2 emissions of Bagnore GPPs normalized to the reservoir area, 45 t/d km^2, summed to deep and background CO_2 for the same area, 109 t/d km^2, are equal to the mean values of the undisturbed areas (110 t/d km^2). The same value is obtained for the Piancastagnaio area.

7. Conclusions

These data demonstrate that the AVGA is a good example of the replacement mechanism operated by the CO_2 carried by deep wells from the reservoir to the surface. The strong reduction observed between 50% and 70% of natural soil gas flux compared to the emissions in greenfield areas is balanced by the gas emission of GPPs. Thus, gases drained with geothermal fluids by wells by the deep reservoirs reduce the natural soil gas emissions.

These results imply a key reflection: i.e., the GPPs emissions reduce up to 50% of the natural emissions in the Mt. Amiata geothermal fields. However, this assumes that comparing the emissions in the brownfields and greenfields of the same geothermal system is the correct procedure. If the reduction of natural emissions is perfectly balanced by the emissions of the power plants, the geothermal production of electricity has zero CO_2 emissions. If the reduction of natural emissions is not counterbalanced by the emissions of the power plants, the practice of reinjection progressively reduces the gas/water vapor ratio in the geothermal reservoirs and then the geothermal generation will yield an environmental bonus by producing electricity that also reduces global CO_2 emissions.

The data presented show that CO_2 (naturally produced in the earth's crust and lithosphere through magmatic and metamorphic processes) because of its physicochemical characteristics is not retained in depth by surface geological formations that are not sufficiently impermeable to gases and is emitted on the Earth's surface. This implies that CO_2 is and would always be emitted to the surface at a constant rate like in the AVGA case study area. The concept of innovative zero-emission power plants currently proposed, implying the compression and reinjection of CO_2, are therefore useless. The compressed and reinjected CO_2 would be enriched in the geothermal reservoirs, reach saturation in the aqueous fluids in reservoirs, and consequently be released back to the surface both by diffuse soil emission and by the increased in gas content in the geothermal fluids. Finally, the concept of CO_2 emissions from GPPs as expressed in g/kWh, must therefore be appropriately reconsidered because the study highlighted that in the Mt. Amiata area, and probably throughout the world, the natural emission of CO_2 in volcanic geothermal areas can exceed the emission from GPPs by at least an order of magnitude. In the AVGA, GPPs contribute only 7.9% to the total CO_2 budget in the atmosphere, and emissions are much lower than those of fossil-fuel power plants, In addition, the amount of gas emitted by GPPs is equivalent to the depletion in natural soil emission, as shown in this study, with a further consequence that the GPPs emission is substituted by an equivalent depletion of natural emission with a zero-emission balance.

Supplementary Materials: The following are available online at www.mdpi.com/article/10.3390/en14154692/s1, Table S1: CO_2 soil flux data.

Author Contributions: Conceptualization, A.S. and A.L.; Methodology, A.S., A.L. and M.P.; Validation, P.M.; Formal Analysis, A.S., A.L., M.S. and V.C.; Investigation, M.S. and V.C.; Software, M.S. and V.C.; Writing—Original Draft Preparation, A.S.; Writing—Review & Editing, A.S., A.L., M.P., R.G., M.S., V.C. and P.M.; Visualization, A.L., M.S. and V.C; Supervision, A.S., A.L. and P.M.; Funding Acquisition A.L. and M.P. All authors have read and agreed to the published version of the manuscript.

Funding: This work was financially supported by University of Pisa and Enel Green Power.

Acknowledgments: The authors are grateful to three anonymous reviewers for their constructive comments and suggestions that helped to improve the quality of the manuscript.

Data Availability Statement: The data presented in this study are available in Table S1.

Conflicts of Interest: The authors declare no conflict of interest.

References

1. Ferrari, R.; Conticelli, S.; Burlamacchi, L.; Manetti, P. Volcanological evolution of the Monte Amiata, Southern Tuscany: New geological and petrochemical data. *Acta Vulcanol.* **1996**, *8*, 41–56.
2. Laurenzi, M.A.; Braschi, E.; Casalini, M.; Conticelli, S. New ^{40}Ar-^{39}Ar dating and revision of the geochronology of the Monte Amiata Volcano, Central Italy. *Ital. J. Geosci.* **2015**, *134*, 255–265, doi:10.3301/IJG.2015.11.
3. Calcagnile, G.; Panza, G.F. The main characteristics of the lithosphere–asthenosphere system in Italy and surrounding regions. *Pure Appl. Geophys.* **1981**, *119*, 865–879.
4. Carmignani, L.; Decandia, F.A.; Disperati, L.; Fantozzi, P.L.; Lazzarotto, A.; Liotta, D.; Meccheri, M. Tertiary extensional tectonics in Tuscany (Northern Apenines Italy). *Tectonophysics* **1994**, *238*, 295–315, doi:10.1016/0040-1951(94)90061-2.
5. Liotta, D. Analisi del settore centro-meridionale del bacino pliocenico di Radicofani (Toscana Meridionale). *Boll. Soc. Geol. Ital.* **1996**, *115*, 115–143.
6. Gianelli, G.; Puxeddu, M.; Batini, F.; Bertini, G.; Dini, I.; Pandeli, E.; Nicolich, R. Geological model of a young volcano-plutonic system: The geothermal region of Monte Amiata (Tuscany, Italy). *Geothermics* **1988**, *17*, 719–734, doi:10.1016/0375-6505(88)90033-8.
7. Ceroti, M.; Fiordelisi, A.; Fulignati, P.; Marianelli, P.; Sbrana, A.; Scazzola, S. Integrated Approach for a successful geothermal wells location in the Monte Amiata area (Southern Tuscany). In Proceedings of the World Geothermal Congress, Melbourne, Australia, 19–25 April 2015; pp. 1–9.
8. Girolami, C.; Barchi, M.R.; Heyde, I.; Pauselli, C.; Vetere, F.; Cannata, A. The Gravity anomaly of Mount Amiata; Different approaches for understanding anomaly source distribution. *Geophys. J. Int.* **2017**, *211*, 865–882, doi:10.1093/gji/ggx350.
9. Brogi, A.; Fabbrini, L.; Liotta, D. Sb-Hg ore deposit distribution controlled by brittle structures: The case of the Selvena mining district (Monte Amiata, Tuscany, Italy). *Ore Geol. Rev.* **2011**, *41*, 35–48, doi:10.1016/j.oregeorev.2011.06.004.
10. Vaselli, O.; Higueras, P.; Nisi, B.; Esbrì, J.M.; Cabassi, J.; Martìnez-Coronado, A.; Tassi, F.; Rappuoli, D. Distribution of gaseous Hg in the Mercury mining district of Mt. Amiata (Central Italy): A geochemical survey prior the reclamation project. *Environ. Res.* **2013**, *125*, 179–187, doi:10.1016/j.envres.2012.12.010.
11. Della Vedova, B.; Bellani, S.; Pellis, G.; Squarci, P. Deep temperatures and surface heat flow distribution. In *Anatomy of an Orogen the Apennines and Adjacent Mediterranean Basins*; Vai, G.B., Martini, I.P., Eds.; Springer: Dordrecht, The Netherlands, 2001; pp. 65–76, ISBN 978-94-015-9829-3.
12. Calamai, A.; Cataldi, R.; Squarci, P.; Taffi, L. Geology, geophysics and hydrogeology of the Monte Amiata geothermal fields. *Geothermics* **1970**, *1*, 1–95.
13. ARPAT (Tuscany Regional Agency for Environmental Protection), Monitoraggio Delle Aree Geotermiche Toscane—Anno 2018 (Monitoring of Geothermal Areas in Tuscany, 2018). Available online: http://www.arpat.toscana.it/documentazione/report/report-geotermia/monitoraggio-delle-aree-geotermiche-toscane-anno-2018 (accessed on 10 June 2021).
14. Minissale, A.; Magro, G.; Vaselli, O.; Verrucchi, C.; Perticone, I. Geochemistry of water and gas discharges from the Mt. Amiata silicic complex and surrounding areas central Italy. *J. Volcanol. Geotherm. Res.* **1997**, *79*, 223–251, doi:10.1016/S0377-0273(97)00028-0.
15. Frondini, F.; Caliro, S.; Cardellini, C.; Chiodini, G.; Morgantini, N. Carbon dioxide degassing and thermal energy release in the Monte Amiata volcanic-geothermal area (Italy). *Appl. Geochem.* **2009**, *24*, 860–875, doi:10.1016/j.apgeochem.2009.01.010.
16. Sbrana, A.; Marianelli, P.; Belgiorno, M.; Sbrana, M.; Ciani, V. Natural CO_2 degassing in the Mount Amiata volcanic–geothermal area. *J. Volcanol. Geotherm. Res.* **2020**, *397*, 106852, doi:10.1016/j.jvolgeores.2020.106852.
17. Marroni, M.; Moratti, G.; Costantini, A.; Conticelli, S.; Benvenuti, M.G.; Pandolfi, L.; Bonini, M.; Cornamusini, G.; Laurenzi, M.A. Geology of the Monte Amiata region, Southern Tuscany, Central Italy. *Italian J. Geosci.* **2015**, *134*, 171–199, doi:10.3301/IJG.2015.13.
18. Barelli, A.; Ceccarelli, A.; Dini, I.; Fiordelisi, A.; Giorgi, N.; Lovari, F.; Romagnoli, P. A Review of the Mt. Amiata Geothermal System (Italy). In Proceedings of the World Geothermal Congress, Bali, Indonesia, 25–29 April 2010.

19. Dini, I.; Ceccarelli, A.; Brogi, A.; Giorgi, N.; Galleni, P.; Rossi, L. Geological Evaluation of the Base of the Mt. Amiata Volcanic Complex (Tuscany, Italy). In Proceedings of the World Geothermal Congress, Bali, Indonesia, 25–29 April 2010.
20. Fulignati, P.; Marianelli, P.; Sbrana, A.; Ciani, V. 3D geothermal modelling of the Mount Amiata hydrothermal system in Italy. *Energies* **2014**, *7*, 7434–7453, doi:10.3390/en7117434.
21. Bertini, G.; Cappetti, G.; Dini, I.; Lovari, F. Deep drilling results and updating of geothermal knowledge on the Mount Amiata area. In Proceedings of the World Geothermal Congress, Florence, Italy, 18–31 May 1995; pp. 1283–1286.
22. Orlando, L.; Bernabini, M.; Bertini, G.; Cameli, G.M.; Dini, I. Interpretazione preliminare del minimo gravimetrico del Monte Amiata. *Studi Geol. Camerti* **1994**, *1*, 175–181.
23. Gianelli, G.; Ruggieri, G.; Mussi, M. Isotopic and fluid inclusion study of hydrothermal and metamorphic carbonates in the Larderello geothermal field and surrounding areas, Italy. *Geothermics* **1997**, *26*, 393–417, doi:10.1016/S0375-6505(97)00001-1.
24. Liotta, D.; Ranalli, G. Correlation between seismic reflectivity and rheology in extended lithosphere: Southern Tuscany, inner Northern Apennines, Italy. *Tectonophysics* **1999**, *315*, 109–122, doi:10.1016/S0040-1951(99)00292-9.
25. Brogi, A. The structure of the Monte Amiata volcano-geothermal area (Northern Apennines, Italy): Neogene-Quaternary compression versus extension. *Int. J. Earth Sci.* **2008**, *97*, 677–703, doi:10.1007/s00531-007-0191-1.
26. Bertini, G.; Casini, M.; Gianelli, G.; Pandeli, E. Geological structure of a long living geothermal system, Larderello, Italy. *Terra Nova* **2006**, *18*, 163–169, doi:10.1111/j.1365-3121.2006.00676.x.
27. Carella, M.; Fulignati, P.; Musumeci, G.; Sbrana, A. Metamorphic consequences of Neogene thermal anomaly in the northern Apennines (Radicondoli-Travale area, Larderello geothermal field—Italy). *Geodinamica Acta* **2000**, *13*, 345–366, doi:10.1016/S0985-3111(00)01051-2.
28. D'Amore, F.; Fancelli, R.; Saracco, L.; Truesdell, A. Gas geothermometry based on CO content: Application to Italian geothermal fields. In Proceedings of the 12th Workshop on Geothermal Reservoir Engineering, Stanford, CA, USA, 20–22 January 1987; pp. 247–252.
29. Gasparrini, M.; Ruggieri, G.; Brogi, A. Diagenesis versus hydrothermalism and fluid–rock interaction within the Tuscan Nappe of the Monte Amiata CO_2-rich geothermal area (Italy). *Geofluids* **2013**, *13*, 159–179, doi:10.1111/gfl.12025.
30. ENEL, ENI-AGIP, CNR and ENEA with the Coordination of the Ministry, 1988, Geothermal Resources National Inventory, Law December 9, 1986 n.896, Repealed by Legislative Decree February 11, 2010 n.22. Available online: https://unmig.mise.gov.it/index.php/it/dati/risorse-geotermiche/inventario-delle-risorse-geotermiche-nazionali (accessed on 10 June 2021).
31. Frondini, F.; Caliro, S.; Cardellini, C.; Chiodini, G.; Morgantini, N.; Parello, F. Carbon dioxide degassing from Tuscany and Northern Latium (Italy). *Global Planet. Change* **2008**, *61*, 89–102, doi:10.1016/j.gloplacha.2007.08.009.
32. Doveri, M.; Nisi, B.; Cerrina Feroni, A.; Ellero, A.; Menichini, M.; Lelli, M.; Masetti, G.; Da Prato, S.; Principe, C.; Raco, B. Geological, hydrodynamic and geochemical features of the volcanic aquifer of Mt. Amiata (Tuscany, Central Italy): An overview. *Acta Vulcanol.* **2012**, *23*, 51–72.
33. Barazzuoli, P.; Bosco, G.; Nante, N.; Rappuoli, D.; Salleolini, M. The aquifer of Mount Amiata: Evaluation of perennial yields its quality. *Mem. Soc. Geol. Ital.* **1994**, *48*, 825–832.
34. Chiodini, G.; Cardellini, C.; Amato, A.; Boschi, E.; Caliro, S.; Frondini, F.; Ventura, G. Carbon dioxide Earth degassing and seismogenesis in central and southern Italy. *J. Geophys. Res.* **2004**, *31*, doi:10.1029/2004GL019480.
35. Vaselli, O.; Cuccoli, F.; Buccianti, A.; Nisi, B.; Lognoli, E.; Lombardi, L.; Moretti, S.; Capannesi, L.; Ramaldi, E.; Tassi, F.; et al. Le emanazioni gassose nel Comune di Castiglione d'Orcia, Final Report of the Agreement between the Department of Earth Sciences of Florence and the Civil Protection of Tuscany, Florence, Italy, July 2006, 120p.
36. Nisi, B.; Vaselli, O.; Tassi, F.; de Elio, J.; Ortega, M.; Caballero, J.; Rappuoli, D.; Mazadiego, L.F. Origin of the gases released from the Acqua Passante and Ermeta wells (Mt. Amiata, central Italy) and possible environmental implications for their closure. *Annal. Geophys.* **2014**, *57*, S0438, doi:10.4401/ag-6584.
37. Lenzi, A.; Caprai, A. Emissioni naturali di idrogeno solforato nell'area amiatina parte I: Prospezioni. In Proceedings of the CODICE ARMONICO 2016, Castiglioncello, Italy, 13–15 October 2016; Volume 6.
38. Lenzi, A.; Caprai, A. Emissioni naturali di idrogeno solforato nell'area amiatina parte II: Misure. In Proceedings of the CODICE ARMONICO 2016, Castiglioncello, Italy, 13–15 October 2016; Volume 6.
39. MaGa, Mapping Gas Emissions. Available online: http://www.magadb.net/ (accessed on 10 June 2021).
40. Brogi, A.; Fabbrini, L. Extensional and strike-slip tectonics across the Monte Amiata–Monte Cetona transect (Northern Apennines, Italy) and seismotectonic implications. *Tectonophysics* **2009**, *476*, 195–209, doi:10.1016/j.tecto.2009.02.020.
41. Brogi, A.; Liotta, D.; Meccheri, M.; Fabbrini, L. Transtensional shear zones controlling volcanic eruptions: The Middle Pleistocene Mt. Amiata volcano (inner Northern Apennines, Italy). *Terra Nova* **2010**, *22*, 137–146, doi:10.1111/j.1365-3121.2010.00927.x.
42. Orlando, A.; Conte, A.M.; Borrini, D.; Perinelli, C.; Gianelli, G.; Tassi, F. Experimental investigation of CO_2-rich fluids production in a geothermal area: The Mt. Amiata (Tuscany, Italy) case study. *Chem. Geol.* **2010**, *274*, 177–186, doi:10.1016/j.chemgeo.2010.04.005.
43. D'Amore, F.; Panichi, C. Evaluation of deep temperatures of hydrothermal systems by a new gas geothermometer. *Geochim. Cosmochim. Acta* **1980**, *44*, 549– 556, doi:10.1016/0016-7037(80)90051-4.
44. Chiodini, G.; Baldini, A.; Barberi, F.; Carapezza, M.L.; Cardellini, C.; Frondini, F.; Granieri, D.; Ranaldi, M. Carbon dioxide degassing at Latera caldera (Italy): Evidence of geothermal reservoir and evaluation of its potential energy. *J. Geophys. Res.* **2007**, *112(B12)*, doi:10.1029/2006JB004896.

45. Madsen, R.; Xu, L.; Claassen, B.; Mc Dermitt, D. Surface Monitoring Method for Carbon Capture and Storage Projects. *Energy Procedia* **2009**, *1*, 2161–2168, doi:10.1016/j.egypro.2009.01.281.
46. Chiodini, G.; Cioni, R.; Guidi, M.; Marini, L.; Raco, B. Soil CO_2 flux measurements in volcanic and geothermal areas. *Appl. Geochem.* **1998**, *13*, 543–552, doi:10.1016/S0883-2927(97)00076-0.
47. Licor Bioscience. *LI-8100 Automated Soil CO_2 Flux System & LI-8150 Multiplexer Instruction Manual*; LI-COR Inc.: Lincoln, NE, USA, 2010.
48. Sinclair, A.J. Selection of threshold values in geochemical data using probability graphs. *J. Geochem. Explor.* **1974**, *3*, 129–149, doi:10.1016/0375-6742(74)90030-2.
49. Cardellini, C.; Chiodini, G.; Frondini, F. Application of stochastic simulation to CO_2 flux from soil: Mapping and quantification of gas release. *J. Geophys. Res.* **2003**, *108*, doi:10.1029/2002JB002165.
50. David, M. *Geostatistical ore reserve estimation (Developments in Geomathematics 2)*; Elsevier: New York, NY, USA, 1977.
51. Remy, N.; Boucher, A.; Wu, J. *Applied Geostatistics with SGeMS: A User's Guide*; Cambridge University Press: Cambridge, UK, 2009.
52. Bertani, R.; Thain, I. Geothermal power generating plant CO_2 emission survey. *IGA News* **2002**, *49*, 1–3.
53. Óladóttir, A.A.; Fridriksson, T.H. The Evolution of CO_2 Emissions and Heat Flow through Soil since 2004 in the Utilized Reykjanes Geothermal Area, SW Iceland: Ten Years of Observations on Changes in Geothermal Surface Activity. In Proceedings of the World Geothermal Congress, Melbourne, Australia, 19–25 April 2015.
54. Ármansson, H. CO_2 emission from Geothermal Plants. In Proceedings of the International Geothermal Conference, Reykjavík, Iceland, 14-17 September 2003; Session #12.
55. Manzella, A.; Serra, D.; Cesari, G.; Bargiacchi, E.; Cei, M.; Cerutti, P.; Conti, P.; Giudetti, G.; Lupi, M.; Vaccaro, M. Geothermal Energy Use, Country Update for Italy. In Proceedings of the European Geothermal Congress, Den Haag, The Netherlands, 11–14 June 2019.
56. GSE (Gestore dei Servizi Energetici). *Statistical Report 2018: Energy from Renewables in Italy*; Edizioni GSE: Roma, Italy, 2019; pp. 101–105.
57. ARPAT (Tuscany Regional Agency for Environmental Protection). Monitoraggio delle Aree Geotermiche Toscane—Anno 2016 (Monitoring of Geothermal Areas in Tuscany, 2016). Available online: http://www.arpat.toscana.it/documentazione/report/report-geotermia/monitoraggio-delle-aree-geotermiche-toscane-anno-2016 (accessed on 10 June 2021).
58. ARPAT (Tuscany Regional Agency for Environmental Protection). Monitoraggio delle Aree Geotermiche Toscane—Anno 2014 (Monitoring of Geothermal Areas in Tuscany, 2014). Available online: http://www.arpat.toscana.it/documentazione/report/report-geotermia/monitoraggio-delle-aree-geotermiche-toscane-anno-2014 (accessed on 10 June 2021).
59. Bravi, M.; Basosi, R. Environmental impact of electricity from selected geothermal power plants in Italy. *J. Clean. Prod.* **2014**, *66*, 301–308, doi:10.1016/j.jclepro.2013.11.015.
60. Ferrara, N.; Parisi, M.L.; Basosi, R. Emissions data from geothermal energy exploitation in Italy. Mendeley Data V1, 2019. Available online: https://data.mendeley.com/datasets/gvpy69796n/1 (accessed on 29 July 2021).
61. Conti, P.; Cei, M.; Razzano, F. Geothermal Energy Use, Country Update for Italy (2010–2015). In Proceedings of the European Geothermal Congress, Strasbourg, France, 19–24 September 2016.
62. ISPRA, Istituto Superiore per la Protezione e la Ricerca Ambientale. Fattori di Emissione Atmosferica di Gas a Effetto Serra nel Settore Elettrico Nazionale e Nei Principali Paesi Europei; Report n. 303/2019; ISPRA: Rome, Italy, 2019; ISBN: 978-88-448-0945-4.
63. Enel Green Power. Dichiarazione Ambientale anni 2017–2019, Dati Relativi All'anno 2016 Per Gli Impianti di Produzione di Energia Elettrica da Fonti Rinnovabili di Enel Green Power S.p.A. Geotermia Italia. Available online: https://corporate.enel.it/content/dam/enel-it/progetti/documenti/impianti-emas-geotermici/ItaliaEnelGreenPower/Dichiarazione-Ambientale-2017.pdf (accessed on 10 June 2021).
64. Orkustofnun, National Energy Authority, Data Repository. Available online: http://www.os.is/orkustofnun/gagnasofn/talnaefni (accessed on 10 June 2021).
65. Fridriksson, T.; Merino, A.M.; Orucu, A.Y.; Audinet, P. Greenhouse gas emissions from geothermal power production. In Proceedings of the 42nd Workshop on Geothermal Reservoir Engineering, Stanford University, Stanford, CA, USA, 13–15 February 2017.
66. Yuniarto, T.E.B.S.; Heviati, E. Geothermal Power Plant Emissions in Indonesia. In Proceedings of the World Geothermal Congress Melbourne, Australia, 19–25 April 2015.
67. Bloomfield, K.K.; Moore, J.N.; Neilson, R.N. Geothermal energy reduces greenhouse gases. *Geotherm. Resour. Counc. Bull.* **2003**, *32*, 77–79.
68. US DoE (U.S. Department of Energy). The Energy Information Administration (EIA), Electric Power Generation and Fuel Consumption, 1989–2010. Power Plants Generation Report and Emissions From Energy Consumption for Electricity Generation Report. Available online: https://www.eia.gov/totalenergy/data/annual/index.php (accessed on 10 June 2021).